Registration beyond Points: General Affine Subspace Alignment via Geodesic Distance on Grassmann Manifold

Supplementary Material

7. Proof of Theorems

7.1. Proof of Theorem 1

Proof. We need to show that f satisfies the following two properties of the group action.

$$1.^{\forall}\mathbf{X} \in \mathrm{Gr}(k,n),\ \mathbf{I}\cdot\mathbf{X} = \mathbf{X}\ (Identity)$$
$$2.^{\forall}(\mathbf{X} \in \mathrm{Gr}(k,n),\ \mathbf{T}_1,\mathbf{T}_2 \in SE(n)),\ (\mathbf{T}_1\mathbf{T}_2)\cdot\mathbf{X} = \mathbf{T}_1\cdot(\mathbf{T}_2\cdot\mathbf{X})\ (Compatibility)$$

1. For the identity matrix $\mathbf{I}$, it is straightforward that $\mathbf{I}\cdot\mathbf{X} = \mathbf{X}$, as the rotation matrix is the identity, and the translation is the zero vector:

$$\begin{aligned}\mathbf{I}\cdot(\mathbb{A}+\mathbf{b}) &= (\mathbf{I}\cdot\mathbb{A}) + (\mathbf{I}\mathbf{b} + \mathbf{I}(\mathbf{I}-\mathbf{A}\mathbf{A}^\top)\mathbf{I}^\top\mathbf{0}) \\ &= \mathbb{A}+\mathbf{b}\end{aligned} \tag{16}$$

2. Given two elements of $SE(n)$, $\mathbf{T}_1 = (\mathbf{R}_1,\mathbf{t}_1)$ and $\mathbf{T}_2 = (\mathbf{R}_2,\mathbf{t}_2)$, $\mathbf{T}_1\cdot(\mathbf{T}_2\cdot\mathbf{X})$ is derived by following process:

$$\mathbf{T}_2\cdot\mathbf{X} = (\mathbf{R}_2\cdot\mathbb{A}) + \mathbf{R}_2\mathbf{b} + \mathbf{R}_2(\mathbf{I}-\mathbf{A}\mathbf{A}^\top)\mathbf{R}_2^\top\mathbf{t}_2 \tag{17}$$
$$\mathbf{T}_1\cdot(\mathbf{T}_2\cdot\mathbf{X}) = \mathbf{R}_1\cdot(\mathbf{R}_2\cdot\mathbb{A}) + \mathbf{R}_1(\mathbf{R}_2\mathbf{b} + \mathbf{R}_2(\mathbf{I}-\mathbf{A}\mathbf{A}^\top)\mathbf{R}_2^\top\mathbf{t}_2) + \mathbf{R}_1(\mathbf{I}-\mathbf{R_2}\mathbf{A}(\mathbf{R_2}\mathbf{A})^\top)\mathbf{R}_1^\top\mathbf{t}_1 \tag{18}$$
$$= \mathbf{R}_1\cdot(\mathbf{R}_2\cdot\mathbb{A}) + \mathbf{R}_1\mathbf{R}_2(\mathbf{b} + (\mathbf{I}-\mathbf{A}\mathbf{A}^\top)(\mathbf{R}_2^\top\mathbf{t}_2 + \mathbf{R}_2^\top\mathbf{R}_1^\top\mathbf{t}_1))\ (\because \mathbf{I} = \mathbf{R}_2\mathbf{R}_2^\top). \tag{19}$$
$$= ((\mathbf{R}_1\mathbf{R}_2)\cdot\mathbb{A}) + \mathbf{R}_1\mathbf{R}_2\mathbf{b} + \mathbf{R}_1\mathbf{R}_2(\mathbf{I}-\mathbf{A}\mathbf{A}^\top)(\mathbf{R}_1\mathbf{R}_2)^\top(\mathbf{R}_1\mathbf{t}_2+\mathbf{t}_1)\ (\because (\mathbf{R}_2\cdot\mathbb{A}) := \mathrm{span}\{\mathbf{R}_2\mathbf{A}\}) \tag{20}$$

Also, since $\mathbf{T}_1\mathbf{T}_2 = (\mathbf{R}_1\mathbf{R}_2, \mathbf{R}_1\mathbf{t}_2+\mathbf{t}_1)$,

$$(\mathbf{T}_2\mathbf{T}_1)\cdot\mathbf{X} = (\mathbf{R_1}\mathbf{R}_2)\cdot\mathbb{A} + \mathbf{R}_1\mathbf{R}_2\mathbf{b} + \mathbf{R}_1\mathbf{R}_2(\mathbf{I}-\mathbf{A}\mathbf{A}^\top)(\mathbf{R}_1\mathbf{R}_2)^\top(\mathbf{R}_1\mathbf{t}_2+\mathbf{t}_1), \tag{21}$$

which is identical to Eq. (20).

□

7.2. Proof of Corollary 1.1

Proof. Assume $\mathbf{x}\in\mathbb{R}^n$ is included in affine subspace $\mathbb{A}+\mathbf{b}$. Then, there exists a unique unit vector $\mathbf{c}$ satisfying

$$\mathbf{x} = \mathbf{A}\mathbf{c} + \mathbf{b}, \tag{22}$$

which represents a coordinate of the point on the plane. Then, by $SE(n)$ transformation, $\mathbf{x}$ moves to

$$\mathbf{x}' = \mathbf{R}\mathbf{A}\mathbf{c} + \mathbf{R}\mathbf{b} + \mathbf{t}. \tag{23}$$

To demonstrate that $\mathbf{x}'$ is included in $\mathbf{T}\cdot(\mathbb{A}+\mathbf{b})$, we need to show that the projection of the difference between $\mathbf{x}'$ and the displacement of $\mathbf{T}\cdot(\mathbb{A}+\mathbf{b})$ onto the orthogonal complement of $\mathbf{R}\cdot\mathbb{A}$ results in the zero vector. This can be proved as follows:

$$(\mathbf{I}-\mathbf{R}\mathbf{A}\mathbf{A}^\top\mathbf{R}^\top)(\mathbf{x}'-\mathbf{b}'(\mathbf{R},\mathbf{t})) = (\mathbf{I}-\mathbf{R}\mathbf{A}\mathbf{A}^\top\mathbf{R}^\top)(\mathbf{R}\mathbf{A}\mathbf{c}+\mathbf{R}\mathbf{b}+\mathbf{t}-\mathbf{R}\mathbf{b}-\mathbf{R}(\mathbf{I}-\mathbf{A}\mathbf{A}^\top)\mathbf{R}^\top\mathbf{t})) \tag{24}$$
$$= (\mathbf{I}-\mathbf{R}\mathbf{A}\mathbf{A}^\top\mathbf{R}^\top)\mathbf{R}\mathbf{A}(\mathbf{c}+\mathbf{A}^\top\mathbf{R}^\top\mathbf{t}) \tag{25}$$
$$= \mathbf{0}.$$

□

7.3. Proof of Theorem 2

Proof. ($\rightarrow$) Given two elements of the Grassmannian, $\mathbb{A} \in \mathrm{Gr}(k,n)$ and $\mathbb{B} \in \mathrm{Gr}(l,n)$, where $k \leq l < n$ are positive integers, assume that every basis vector of $\mathbb{A}$, denoted as $\mathbf{a}_i$ $(i = 1, \cdots, k)$, is spanned by the basis vectors of $\mathbb{B}$, denoted as $\mathbf{b}_i$ $(i = 1, \cdots, l)$. In this case, each $\mathbf{a}_i$ can be represented as:

$$\mathbf{a}_i = \sum_{j=1}^{l} c_{ij}\mathbf{b}_j \tag{26}$$

This leads to orthonormal basis representation of $\mathbb{A}$ as:

$$\mathbf{A} = \begin{bmatrix} \sum_{j=1}^{l} c_{1j}\mathbf{b}_j & \cdots & \sum_{j=1}^{l} c_{kj}\mathbf{b}_j \end{bmatrix} = \begin{bmatrix} c_{11}\mathbf{b}_1 & \cdots & c_{k1}\mathbf{b}_1 \end{bmatrix} + \cdots + \begin{bmatrix} c_{1l}\mathbf{b}_l & \cdots & c_{kl}\mathbf{b}_l \end{bmatrix}. \tag{27}$$

By multiplying the orthonormal basis matrix of $\mathbb{B}$, which is $\mathbf{B} = \begin{bmatrix} \mathbf{b}_1 & \cdots & \mathbf{b}_l \end{bmatrix}$, to the $\mathbf{A}^\top$, we obtain following matrix $\mathbf{A}^\top\mathbf{B} \in \mathbb{R}^{k\times l}$:

$$\mathbf{A}^\top\mathbf{B} = \begin{bmatrix} c_{11} & \cdots & c_{1l} \\ \vdots & \ddots & \vdots \\ c_{k1} & \cdots & c_{kl} \end{bmatrix}. \tag{28}$$

Since every $\mathbf{a}_i$ is an orthonormal matrix, we have the following two conditions:

$$c_{i1}^2 + c_{i2}^2 + \cdots + c_{il}^2 = 1, \ (i = 1, \ldots, k) \tag{29}$$

$$\sum_{j=1}^{l} c_{ij}c_{i'j} = 0 \ (\forall i, i' \in \{1, \ldots, k\}, \ i \neq i'). \tag{30}$$

This implies that $\mathbf{A}^\top\mathbf{B}$ consists of k orthonormal row vectors. Since every singular value of an orthonormal matrix is 1, all principal angles are equal to zero by Eq. (38), resulting in a Grassmann distance of zero.

($\leftarrow$) Given two elements of the Grassmannian, $\mathbb{A} \in \mathrm{Gr}(k,n)$ and $\mathbb{B} \in \mathrm{Gr}(l,n)$, where $k \leq l < n$ are positive integers, assume that the Grassmann distance between them is zero. Then, for every principal vector pair $(\mathbf{p}_i, \mathbf{q}_i)$ $(i = 1, \ldots, k)$, the condition $\mathbf{p}_i = \mathbf{q}_i$ is satisfied. According to Definition 5, these principal vectors constitute the first k orthonormal basis vectors of both $\mathbb{A}$ and $\mathbb{B}$. Therefore, every basis vector of $\mathbb{A}$ is spanned by the basis vectors of $\mathbb{B}$. □

7.4. Proof of Problem 2

Given two elements of the affine Grassmannian, $\mathbb{A} + \mathbf{c} \in \mathrm{Graff}(k,n)$ and $\mathbb{B} + \mathbf{d} \in \mathrm{Graff}(l,n)$, where $k \leq l < n$ are positive integers, we need to show that every basis vector of $z(\mathbb{A} + \mathbf{c})$ is spanned by the basis vectors of $z(\mathbf{T} \cdot (\mathbb{B} + \mathbf{d}))$ if and only if the following condition is satisfied:

$$\sum_{i=1}^{k} \|\mathbf{P}_{\mathbf{R}\cdot\mathbb{B}}\mathbf{a}_i - \mathbf{a}_i\|_2^2 + \left\|\mathbf{P}_{z(\mathbf{T}\cdot(\mathbb{B}+\mathbf{d}))}\tilde{\mathbf{c}} - \tilde{\mathbf{c}}\right\|_2^2 = 0. \tag{31}$$

Proof. ($\rightarrow$) The orthonormal basis matrix of each embedded subspace is represented as:

$$\mathbf{Y}_{z(\mathbb{A}+\mathbf{c})} = \begin{bmatrix} \mathbf{a}_1 & \ldots & \mathbf{a}_k & \frac{\mathbf{c}}{\sqrt{1+\|\mathbf{c}\|^2}} \\ 0 & \ldots & 0 & \frac{1}{\sqrt{1+\|\mathbf{c}\|^2}} \end{bmatrix}, \ \mathbf{Y}_{z(\mathbf{T}\cdot(\mathbb{B}+\mathbf{d}))} = \begin{bmatrix} \mathbf{R}\mathbf{b}_1 & \ldots & \mathbf{R}\mathbf{b}_l & \frac{\mathbf{d}'(\mathbf{R},\mathbf{t})}{\sqrt{1+\|\mathbf{d}'(\mathbf{R},\mathbf{t})\|^2}} \\ 0 & \ldots & 0 & \frac{1}{\sqrt{1+\|\mathbf{d}'(\mathbf{R},\mathbf{t})\|^2}} \end{bmatrix} \tag{32}$$

Since $\bar{\mathbf{a}}_i = [\mathbf{a}_i^\top \ 0]^\top$ is spanned by the columns of $\mathbf{Y}_{z(\mathbf{T}\cdot(\mathbb{B}+\mathbf{d}))}$, we can write:

$$\bar{\mathbf{a}}_i = \sum_{j=1}^{l} c_{ij}\overline{\mathbf{R}\mathbf{b}}_j + c_{i(l+1)}\tilde{\mathbf{d}}'(\mathbf{R},\mathbf{t}). \tag{33}$$

It is readily shown that $c_{i(l+1)} = 0$ since the last element of $\bar{\mathbf{a}}_i$ is zero. Then, $\mathbf{a}_i$ is a linear combination of $\mathbf{B} = [\mathbf{b}_1 \dots \mathbf{b}_l]$, where $c_{ij} = \mathbf{a}_i^\top \mathbf{R}\mathbf{b}_j$ due to the orthonormality of $\mathbf{RB}$. Rewrite this with linear combination of $\tilde{\mathbf{c}}$:

$$\mathbf{a}_i = \sum_{j=1}^{l} (\mathbf{a}_i^\top \mathbf{R}\mathbf{b}_j)\mathbf{R}\mathbf{b}_j = \mathbf{P}_{\mathbf{R}\cdot\mathbb{B}}\mathbf{a}_i, \tag{34}$$

$$\tilde{\mathbf{c}} = \sum_{j=1}^{l} (\tilde{\mathbf{c}}^\top \overline{\mathbf{R}\mathbf{b}}_j)\overline{\mathbf{R}\mathbf{b}}_j + (\tilde{\mathbf{c}}^\top \tilde{\mathbf{d}}'(\mathbf{R},\mathbf{t}))\tilde{\mathbf{d}}'(\mathbf{R},\mathbf{t}) = \mathbf{P}_{z(\mathbf{T}\cdot(\mathbb{B}_\mathbf{d}))}\tilde{\mathbf{c}}, \tag{35}$$

which is identical to the condition Eq. (31) being satisfied.

($\leftarrow$) Starting from Eq. (31) being satisfied, we also derive Eq. (34) and Eq. (35), which implies that every basis of $z(\mathbb{A}+\mathbf{c})$ is spanned by the bases of $z(\mathbf{T}\cdot(\mathbb{B}+\mathbf{d}))$. □

As a result, to validate whether the bases of another affine subspace span the basis of one affine subspace, we only need to check if Eq. (31) is satisfied. To formulate the cost function for minimizing the geodesic distance, this condition can be utilized by defining the left-hand side as a residual. Summing these residuals over N correspondences yields the cost function for Problem 2.

7.5. Proof of Corollaries

Simply replacing each affine primitive in Problem 2 with 3D lines and planes, as represented in each corollary, provides the result.

8. Derivation Details

8.1. Grassmann Distance

Inducing the geodesic distance on the Grassmannian requires a principal vector and angle defined as follows [42]:

Definition 4 (Principal Vector)**.** *Let $\mathbb{A} \in \mathrm{Gr}(k,n)$, $\mathbb{B} \in \mathrm{Gr}(l,n)$, and $k \leqslant l < n$ be positive integers. Then i^{th} principal vectors $(\mathbf{p}_i, \mathbf{q}_i), i = 1, \cdots, k$, are defined recursively as solutions to the optimization problem:*

$$\begin{aligned} &\max (\mathbf{p}_i^\top \mathbf{q}_i) \ \ \textit{subject to} \\ &\mathbf{p}_i \in \mathbb{A}, \mathbf{p}_i^\top \mathbf{p}_1 = \cdots = \mathbf{p}_i^\top \mathbf{p}_{i-1} = 0, \|\mathbf{p}_i\|_2 = 1, \\ &\mathbf{q}_i \in \mathbb{B}, \mathbf{q}_i^\top \mathbf{q}_1 = \cdots = \mathbf{q}_i^\top \mathbf{q}_{i-1} = 0, \|\mathbf{q}_i\|_2 = 1. \end{aligned} \tag{36}$$

Then, the i^{th} principal angle θ_i is defined by:

$$\cos\theta_i = \mathbf{p}_i^\top \mathbf{q}_i. \tag{37}$$

Principal angles provide a natural measure for obtaining the closeness between two linear subspaces within $\mathbb{R}^n$, spanned by columns of matrices [12, 15]. This is due to its recursive definition, which extends the distance between 1-dimensional linear subspaces—explicitly derived as cosine similarity—to the range spaces of matrices. Derivation of principal angles requires SVD [5]. Let $\mathbf{A}$ and $\mathbf{B}$ be two orthonormal basis matrices of $\mathbb{A} \in \mathrm{Gr}(k,n)$ and $\mathbb{B} \in \mathrm{Gr}(l,n)$. Then, the principal angles are given by:

$$\theta_i = \cos^{-1}\sigma_i, \ i = 1, \cdots, k, \tag{38}$$

where σ_i refers to i^{th} singular value of $\mathbf{A}^\top\mathbf{B}$. Then, the geodesic distance on two elements of Grassmannian, denoted as Grassmann distance is defined as follows:

Definition 5 (Grassmann Distance)**.** *Let $k \leqslant l < n$, and $\theta_1, \cdots, \theta_k$ be the principal angles between $\mathbb{A} \in \mathrm{Gr}(k,n)$ and $\mathbb{B} \in \mathrm{Gr}(l,n)$, then the geodesic distance between $\mathbb{A}$ and $\mathbb{B}$ is given by:*

$$\mathrm{d}_{\mathrm{Gr}}(\mathbb{A},\mathbb{B}) = (\sum_{i=1}^{k} \theta_i^2)^{1/2}. \tag{39}$$

8.2. Displacement Vectors

Given an affine subspace $\mathbb{A} + \mathbf{c} \in \mathrm{Graff}(k, n)$, the unique displacement $\mathbf{c}_0$ of this space is determined as follows:

$$\mathbf{c}_0 = (\mathbf{I} - \mathbf{A}\mathbf{A}^\top)\mathbf{c}. \tag{40}$$

This also represents the displacement and is orthogonal to $\mathbb{A}$ since:

$$\mathbf{A}^\top \mathbf{c}_0 = \mathbf{A}^\top(\mathbf{I} - \mathbf{A}\mathbf{A}^\top)\mathbf{c} = 0, \tag{41}$$

$$\begin{aligned}(\mathbf{I} - \mathbf{A}\mathbf{A}^\top)(\mathbf{c} - \mathbf{c}_0) &= (\mathbf{I} - \mathbf{A}\mathbf{A}^\top)(\mathbf{c} - (\mathbf{I} - \mathbf{A}\mathbf{A}^\top)\mathbf{c}) \\ &= (\mathbf{I} - \mathbf{A}\mathbf{A}^\top)(\mathbf{A}\mathbf{A}^\top\mathbf{c}) \\ &= 0,\end{aligned} \tag{42}$$

where each equation demonstrates the orthogonality of $\mathbf{c}_0$ to $\mathbb{A}$ and the orthogonality of $\mathbf{c} - \mathbf{c}_0$ to the orthogonal complement of $\mathbb{A}$.

8.3. Rotation Search

8.3.1. Line-to-line case

Assume the current rotation cube is $\mathcal{C}_\mathbf{r}$ with a half-side length of σ_r and centered at $\mathbf{R}_0$. An objective function for this case is:

$$\max_{\mathbf{R}\in\mathcal{C}_r} \sum_{i=1}^{N} \mathbf{1}(\epsilon - \mathrm{d}_{\mathrm{Gr}}(\mathbf{R}\mathbf{d}_1^i, \mathbf{d}_2^i)^2). \tag{43}$$

We first derive a lower bound for $\mathrm{d}_{\mathrm{Gr}}(\mathbf{R}\mathbf{d}_1^i, \mathbf{d}_2^i)$ for an arbitrary rotation $\mathbf{R}$ within the cube $\mathcal{C}_\mathbf{r}$ using the triangle inequality of the Grassmann distance:

$$\mathrm{d}_{\mathrm{Gr}}(\mathbf{R}\mathbf{d}_1^i, \mathbf{d}_2^i) \geq \mathrm{d}_{\mathrm{Gr}}(\mathbf{R}_0\mathbf{d}_1^i, \mathbf{d}_2^i) - \mathrm{d}_{\mathrm{Gr}}(\mathbf{R}_0\mathbf{d}_1^i, \mathbf{R}\mathbf{d}_1^i). \tag{44}$$

Then from [40], an upper bound for $\mathrm{d}_{\mathrm{Gr}}(\mathbf{R}_0\mathbf{d}_1^i, \mathbf{R}\mathbf{d}_1^i)$ is written as:

$$\mathrm{d}_{\mathrm{Gr}}(\mathbf{R}_0\mathbf{d}_1^i, \mathbf{R}\mathbf{d}_1^i) \leq \min(\frac{\pi}{2}, \sqrt{3}\sigma_r). \tag{45}$$

From Eq. (44) and Eq. (45), an upper bound for the objective function of Eq. (43) is derived as:

$$\max_{\mathbf{R}\in\mathcal{C}_r} \sum_{i=1}^{N} \mathbf{1}\left(\epsilon - \mathrm{d}_{\mathrm{Gr}}(\mathbf{R}\mathbf{d}_1^i, \mathbf{d}_2^i)^2\right) \leq \sum_{i=1}^{N} \mathbf{1}\left(\epsilon - \max\left(0, \mathrm{d}_{\mathrm{Gr}}(\mathbf{R}_0\mathbf{d}_1^i, \mathbf{d}_2^i) - \min(\frac{\pi}{2}, \sqrt{3}\sigma_r)\right)^2\right) \tag{46}$$

$$:= \bar{\nu}_r. \tag{47}$$

Additionally, a lower bound for the objective function in Eq. (43) is readily derived as:

$$\max_{\mathbf{R}\in\mathcal{C}_r} \sum_{i=1}^{N} \mathbf{1}\left(\epsilon - \mathrm{d}_{\mathrm{Gr}}(\mathbf{R}\mathbf{d}_1^i, \mathbf{d}_2^i)^2\right) \geq \sum_{i=1}^{N} \mathbf{1}\left(\epsilon - \mathrm{d}_{\mathrm{Gr}}(\mathbf{R}_0\mathbf{d}_1^i, \mathbf{d}_2^i)^2\right) \tag{48}$$

$$:= \underline{\nu}_r \tag{49}$$

8.3.2. Line-to-plane case

An objective function for this case is:

$$\max_{\mathbf{R}\in\mathcal{C}_r} \sum_{i=1}^{N} \mathbf{1}\left(\epsilon - \mathrm{d}_{\mathrm{Gr}}(\mathbf{d}^i, \mathbf{P}_{\mathbf{R}\cdot\mathbb{B}^i}\mathbf{d}^i)^2\right). \tag{50}$$

From the triangle inequality, the lower bound of $\mathrm{d}_{\mathrm{Gr}}(\mathbf{d}^i, \mathbf{P}_{\mathbf{R}\cdot\mathbb{B}^i}\mathbf{d}^i)$ is derived as:

$$\mathrm{d}_{\mathrm{Gr}}(\mathbf{d}^i, \mathbf{P}_{\mathbf{R}\cdot\mathbb{B}^i}\mathbf{d}^i) \geq \mathrm{d}_{\mathrm{Gr}}(\mathbf{d}^i, \mathbf{P}_{\mathbf{R}_0\cdot\mathbb{B}^i}\mathbf{d}^i) - \mathrm{d}_{\mathrm{Gr}}(\mathbf{P}_{\mathbf{R}_0\cdot\mathbb{B}^i}\mathbf{d}^i, \mathbf{P}_{\mathbf{R}\cdot\mathbb{B}^i}\mathbf{d}^i). \tag{51}$$

Denote a normal vector of $\mathbb{B}^i$ as $\mathbf{n}^i$, an acute angle between $\mathbf{R}_0\mathbf{n}^i$ and $\mathbf{R}\mathbf{n}^i$ as θ (it is identical to $\mathrm{d}_{\mathrm{Gr}}(\mathbf{R}_0\mathbf{n}^i, \mathbf{R}\mathbf{n}^i)$), and a mid-point of $\mathbf{R}_0\mathbf{n}^i$ and $\mathbf{R}\mathbf{n}^i$ on the arc as $\mathbf{R}_m\mathbf{n}^i$. Then, an upper bound of $\mathrm{d}_{\mathrm{Gr}}(\mathbf{P}_{\mathbf{R}_0\cdot\mathbb{B}^i}\mathbf{d}^i, \mathbf{P}_{\mathbf{R}\cdot\mathbb{B}^i}\mathbf{d}^i)$ can only be explicitly derived under following observation:

$$\text{if } \mathrm{d}_{\mathrm{Gr}}(\mathbf{R}_m\mathbf{n}^i, \mathbf{d}^i) \geq \frac{\theta}{2} \rightarrow \mathrm{d}_{\mathrm{Gr}}(\mathbf{P}_{\mathbf{R}_0\cdot\mathbb{B}^i}\mathbf{d}^i, \mathbf{P}_{\mathbf{R}\cdot\mathbb{B}^i}\mathbf{d}^i) \leq \mathrm{d}_{\mathrm{Gr}}(\mathbf{R}_0\mathbf{n}, \mathbf{R}\mathbf{n}) \leq \min(\frac{\pi}{2}, \sqrt{3}\sigma_r). \tag{52}$$

Extending this observation into $\mathcal{C}_r$, we obtain an upper bound ψ_r within the cube:

$$\psi_r = \begin{cases} \min(\pi/2, \sqrt{3}\sigma_r) & \left(\mathrm{d}_{\mathrm{Gr}}(\mathbf{R}_0\mathbf{n}^i, \mathbf{d}^i) \geq \sqrt{3}\sigma_r\right) \\ \pi/2 & \left(\mathrm{d}_{\mathrm{Gr}}(\mathbf{R}_0\mathbf{n}^i, \mathbf{d}^i) < \sqrt{3}\sigma_r\right) \end{cases} \tag{53}$$

Then, the upper bound of Eq. (50) is derived by substituting ψ_r into Eq. (51):

$$\max_{\mathbf{R}\in\mathcal{C}_r} \sum_{i=1}^{N} \mathbf{1}\left(\epsilon - \mathrm{d}_{\mathrm{Gr}}(\mathbf{d}^i, \mathbf{P}_{\mathbf{R}\cdot\mathbb{B}^i}\mathbf{d}^i)^2\right) \leq \sum_{i=1}^{N} \mathbf{1}\left(\epsilon - \max\left(0, \mathrm{d}_{\mathrm{Gr}}(\mathbf{d}^i, \mathbf{P}_{\mathbf{R}_0\mathbb{B}^i}\mathbf{d}^i) - \psi_r\right)^2\right) \tag{54}$$

$$:= \bar{\nu}_r. \tag{55}$$

A lower bound is derived similarly as *line-to-line* case, which is:

$$\max_{\mathbf{R}\in\mathcal{C}_r} \sum_{i=1}^{N} \mathbf{1}\left(\epsilon - \mathrm{d}_{\mathrm{Gr}}(\mathbf{d}^i, \mathbf{P}_{\mathbf{R}\cdot\mathbb{B}^i}\mathbf{d}^i)^2\right) \geq \sum_{i=1}^{N} \mathbf{1}\left(\epsilon - \mathrm{d}_{\mathrm{Gr}}(\mathbf{d}^i, \mathbf{P}_{\mathbf{R}_0\cdot\mathbb{B}^i}\mathbf{d}^i)^2\right) \tag{56}$$

$$:= \underline{\nu}_r \tag{57}$$

8.3.3. Plane-to-plane case

The same results can be obtained by substituting the direction vectors $\mathbf{d}_1^i$ and $\mathbf{d}_2^i$ with the normal vectors $\mathbf{n}_1^i$ and $\mathbf{n}_2^i$ from Sec. 8.3.1.

8.4. Translation Search

8.4.1. Line-to-line case

Assume the current translation cube is $\mathcal{C}_\mathbf{t}$, with the center at $\mathbf{t}_0$ and vertices denoted as $\mathcal{V}_t$. An objective function for this case is:

$$\min_{\mathbf{t}\in\mathcal{C}_t} \sum_{i=1}^{N} \left\| \mathbf{P}_{z(\mathbf{T}\cdot l_1^i)}\tilde{\mathbf{b}}_2^i - \tilde{\mathbf{b}}_2^i \right\|_2^2, \tag{58}$$

where $\mathbf{T} = (\mathbf{R}^*, \mathbf{t})$ and $\mathbf{P}_{z(\mathbf{T}\cdot l_1^i)}\mathbf{b}_2^i = \left((\tilde{\mathbf{b}}_2^i)^\top \overline{\mathbf{R}^*\mathbf{d}_1^i}\right)\overline{\mathbf{R}^*\mathbf{d}_1^i} + \left((\tilde{\mathbf{b}}_2^i)^\top \tilde{\mathbf{b}}_1'^i(\mathbf{R}^*, \mathbf{t})\right)\tilde{\mathbf{b}}_1'^i(\mathbf{R}^*, \mathbf{t})$. Then, from the triangle inequality of Euclidean distance, lower bound of $\left\| \mathbf{P}_{z(\mathbf{T}\cdot l_1^i)}\tilde{\mathbf{b}}_2^i - \tilde{\mathbf{b}}_2^i \right\|_2$ is:

$$\left\| \mathbf{P}_{z(\mathbf{T}\cdot l_1^i)}\tilde{\mathbf{b}}_2^i - \tilde{\mathbf{b}}_2^i \right\|_2 \geq \left\| \mathbf{P}_{z(\mathbf{T}_0\cdot l_1^i)}\tilde{\mathbf{b}}_2^i - \tilde{\mathbf{b}}_2^i \right\|_2 - \left\| \mathbf{P}_{z(\mathbf{T}_0\cdot l_1^i)}\tilde{\mathbf{b}}_2^i - \mathbf{P}_{z(\mathbf{T}\cdot l_1^i)}\tilde{\mathbf{b}}_2^i \right\|_2, \tag{59}$$

where $\mathbf{T}_0 = (\mathbf{R}^*, \mathbf{t}_0)$. From its definition, $\left\| \mathbf{P}_{z(\mathbf{T}_0\cdot l_1^i)}\tilde{\mathbf{b}}_2^i - \mathbf{P}_{z(\mathbf{T}\cdot l_1^i)}\tilde{\mathbf{b}}_2^i \right\|_2$ can be rewritten as:

$$\left\| \mathbf{P}_{z(\mathbf{T}_0\cdot l_1^i)}\tilde{\mathbf{b}}_2^i - \mathbf{P}_{z(\mathbf{T}\cdot l_1^i)}\tilde{\mathbf{b}}_2^i \right\|_2 = \left\| \left((\tilde{\mathbf{b}}_2^i)^\top \tilde{\mathbf{b}}_1'^i(\mathbf{R}^*, \mathbf{t}_0)\right)\tilde{\mathbf{b}}_1'^i(\mathbf{R}^*, \mathbf{t}_0) - \left((\tilde{\mathbf{b}}_2^i)^\top \tilde{\mathbf{b}}_1'^i(\mathbf{R}^*, \mathbf{t})\right)\tilde{\mathbf{b}}_1'^i(\mathbf{R}^*, \mathbf{t}) \right\|_2. \tag{60}$$

Recall that from Theorem 3:

$$\mathbf{b}_1'^i(\mathbf{R}^*, \mathbf{t}) = \mathbf{R}^*\mathbf{b}_1^i + \mathbf{R}^*(\mathbf{I} - \mathbf{d}\mathbf{d}^\top)\mathbf{R}^{*\top}\mathbf{t}. \tag{61}$$

Since $\mathbf{t} \in \mathcal{C}_t$, a set of vectors $\mathbf{b}_1'^i(\mathbf{R}^*, \mathbf{t})$ forms a line segment within $\mathbb{R}^3$, where its two end-points are always formulated from $\mathbf{t} \in \mathcal{V}_t$. Augmenting the last element with 1 and normalizing to make $\tilde{\mathbf{b}}_1'^i(\mathbf{R}^*, \mathbf{t})$, the set is now mapped to an arc on 3-sphere in $\mathbb{R}^4$, and the two end-points of the arc $\mathbf{v}_1$ and $\mathbf{v}_2$ are maintained, which means $\mathbf{v}_1, \mathbf{v}_2 \in \tilde{\mathbf{b}}_1'^i(\mathbf{R}^*, \mathbf{t})$, where $\mathbf{t} \in \mathcal{V}_t$.

Our objective is to obtain an upper bound of Eq. (60). Observe that each term of the right-hand side is multiplied by $\left((\tilde{\mathbf{b}}_2^i)^\top \tilde{\mathbf{b}}_1'^i(\mathbf{R}^*, \mathbf{t}_0)\right)$ and $\left((\tilde{\mathbf{b}}_2^i)^\top \tilde{\mathbf{b}}_1'^i(\mathbf{R}^*, \mathbf{t})\right)$, respectively. These terms represent an inner product between a stationary point on 3-sphere $\tilde{\mathbf{b}}_2^i$ and points on the arc. Starting from $\mathbf{v}_1$ and heading to $\mathbf{v}_2$, we observe that in every tested case in our experiments, where the two endpoints are sufficiently close, these inner product values exhibit only four possible shapes: monotonic increasing, monotonic decreasing, convex, or concave. As a result, we can conclude that Eq. (60) achieves its maximum at one of the vertices, and its value can be expressed as:

$$\psi_t = \max_{\mathbf{t} \in \mathcal{V}_t} \left\| \left((\tilde{\mathbf{b}}_2^i)^\top \tilde{\mathbf{b}}_1'^i(\mathbf{R}^*, \mathbf{t}_0)\right) \tilde{\mathbf{b}}_1'^i(\mathbf{R}^*, \mathbf{t}_0) - \left((\tilde{\mathbf{b}}_2^i)^\top \tilde{\mathbf{b}}_1'^i(\mathbf{R}^*, \mathbf{t})\right) \tilde{\mathbf{b}}_1'^i(\mathbf{R}^*, \mathbf{t}) \right\|_2 \tag{62}$$

Therefore, the lower bound of the objective function is:

$$\min_{\mathbf{t} \in \mathcal{C}_t} \sum_{i=1}^{N} \left\| \mathbf{P}_{z(\mathbf{T} \cdot l_1^i)} \tilde{\mathbf{b}}_2^i - \tilde{\mathbf{b}}_2^i \right\|_2^2 \geq \sum_{i=1}^{N} \left(\max(0, \left\| \mathbf{P}_{z(\mathbf{T}_0 \cdot l_1^i)} \tilde{\mathbf{b}}_2^i - \tilde{\mathbf{b}}_2^i \right\|_2 - \psi_t) \right)^2 \tag{63}$$

$$= \underline{e}_t \tag{64}$$

Also, an upper bound is:

$$\min_{\mathbf{t} \in \mathcal{C}_t} \sum_{i=1}^{N} \left\| \mathbf{P}_{z(\mathbf{T} \cdot l_1^i)} \tilde{\mathbf{b}}_2^i - \tilde{\mathbf{b}}_2^i \right\|_2^2 \leq \sum_{i=1}^{N} \left\| \mathbf{P}_{z(\mathbf{T}_0 \cdot l_1^i)} \tilde{\mathbf{b}}_2^i - \tilde{\mathbf{b}}_2^i \right\|_2^2 \tag{65}$$

$$= \bar{e}_t \tag{66}$$

The process for obtaining the bounds is exactly the same for the case of the *line-to-plane* and *plane-to-plane* cases.

8.5. Algorithms

This section introduces the entire pipeline for solving the *line-to-line* registration problem with our BnB solver. The process for obtaining solutions in *line-to-plane* and *plane-to-plane* registration is analogous; therefore, we omit detailed algorithms for these cases.

Algorithm 2 Optimal 3D Line Registration

Input:
$\mathcal{X} = \{(\mathbf{d}_{t_i}, \mathbf{b}_{t_i})\},\ (i = 1, \cdots, N)$: Target lines
$\mathcal{Y} = \{(\mathbf{d}_{s_j}, \mathbf{b}_{s_j})\},\ (j = 1, \cdots, M)$: Source lines
$\mathcal{C}_{\mathbf{R}}$: Initial $SO(3)$ cube for rotational BnB
$\mathcal{C}_{\mathbf{t}}$: Initial $\mathbb{R}^3$ cube for translational BnB
$\epsilon_{\mathbf{R}}, \epsilon_{\mathbf{t}}$: Threshold for rotational and translational BnB
$\mathcal{I}_i$: Initial correspondences
Output:
$(\mathbf{R}^*, \mathbf{t}^*)$: Optimal transformation
$\mathcal{I}_f$: Resulted correspondences

$\mathcal{X}_{lin}$ = {}, $\mathcal{Y}_{lin}$ = {}
for $i = 1 : N$ **do** % Definition 3
  $\mathcal{X}_{lin}[i][:, 0] \leftarrow \bar{\mathbf{d}}_{t_i}$
  $\mathcal{X}_{lin}[i][:, 1] \leftarrow \tilde{\mathbf{b}}_{t_i}$
end for
for $j = 1 : M$ **do** % Definition 3
  $\mathcal{Y}_{lin}[j][:, 0] \leftarrow \bar{\mathbf{d}}_{s_j}$
  $\mathcal{Y}_{lin}[j][:, 1] \leftarrow \tilde{\mathbf{b}}_{s_j}$
end for
if $\mathcal{I}_i$ is **not** empty **then**
  $\mathcal{I}_f, \mathbf{R}^*$ = `CorrRBnB`$(\mathcal{X}_{lin}, \mathcal{Y}_{lin}, \mathcal{I}_i, \mathcal{C}_{\mathbf{R}}, \epsilon_{\mathbf{R}})$ % Algorithm 3
else
  $\mathcal{I}_f, \mathbf{R}^*$ = `FullRBnB`$(\mathcal{X}_{lin}, \mathcal{Y}_{lin}, \mathcal{C}_{\mathbf{R}}, \epsilon_{\mathbf{R}})$ % Algorithm 4
end if
$\mathbf{t}^*$ = `TBnB`$(\mathcal{X}_{lin}, \mathcal{Y}_{lin}, \mathcal{I}_f, \mathbf{R}^*, \mathcal{C}_{\mathbf{t}}, \epsilon_{\mathbf{t}})$ % Algorithm 5
return $\mathcal{I}_f, \mathbf{R}^*, \mathbf{t}^*$

Algorithm 3 CorrRBnB: Rotation BnB with correspondences

Input:
$\mathcal{X}_{lin} = \{(\bar{\mathbf{d}}_{t_i}, \tilde{\mathbf{b}}_{t_i})\},\ (i = 1, \cdots, N)$: Target embeddings
$\mathcal{Y}_{lin} = \{(\bar{\mathbf{d}}_{s_j}, \tilde{\mathbf{b}}_{s_j})\},\ (j = 1, \cdots, M)$: Source embeddings
$\mathcal{C}_{\mathbf{R}}$: Initial $SO(3)$ search cube
$\epsilon_{\mathbf{R}}$: BnB threshold
$\mathcal{I}_i$: Initial correspondences
Output:
$\mathbf{R}^*$: Optimal rotation
$\mathcal{I}_f$: Resulted correspondences

$\mathcal{I}_f \leftarrow \mathcal{I}_i$
Add initial cube $\mathcal{C}_{\mathbf{R}}$ into priority queue $\mathbf{Q}_{\mathbf{R}}$
while $\mathcal{I}_f.size < \bar{\nu}_r$ **do**
  Read cube $\mathcal{C}_r$ with the greatest upper bound $\bar{\nu}_r$ from $\mathbf{Q}_{\mathbf{R}}$
  for all sub-cube $\mathcal{C}_{r_i}$ **do**
    Compute the lower bound $\underline{\nu}_{r_i}$ % Eq. (48)
    if $\mathcal{I}_f.size < 2\underline{\nu}_{r_i}$ **then**
      $(\mathcal{I}_f, \mathbf{R}^*) \leftarrow$ `LMOptimization`$(\mathcal{X}_{lin}, \mathcal{Y}_{lin}, \mathcal{I}_f, \mathbf{R}^*)$
    end if
    Compute the upper bound $\bar{\nu}_{r_i}$ % Eq. (46)
    if $\mathcal{I}_f.size < \bar{\nu}_{r_i}$ **then**
      Add $\mathcal{C}_{r_i}$ to queue $\mathbf{Q}_{\mathbf{R}}$
    end if
  end for
end while
return $\mathcal{I}_f, \mathbf{R}^*$

Algorithm 4 FullRBnB: Rotation BnB without correspondences

Input:
$\mathcal{X}_{lin} = \{(\bar{\mathbf{d}}_{t_i}, \tilde{\mathbf{b}}_{t_i})\},\ (i = 1, \cdots, N)$: Target embeddings
$\mathcal{Y}_{lin} = \{(\bar{\mathbf{d}}_{s_j}, \tilde{\mathbf{b}}_{s_j})\},\ (j = 1, \cdots, M)$: Source embeddings
$\mathcal{C}_{\mathbf{R}}$: Initial $SO(3)$ search cube
$\epsilon_{\mathbf{R}}$: BnB threshold
Output:
$\mathbf{R}^*$: Optimal rotation
$\mathcal{I}_f$: Resulted correspondences

$\mathcal{I}_f = \{\}$
Add initial cube $\mathcal{C}_{\mathbf{R}}$ into priority queue $\mathbf{Q}_{\mathbf{R}}$
while $\mathcal{I}_f.size < \bar{\nu}_r$ **do**
  Read cube $\mathcal{C}_r$ with the greatest upper bound $\bar{\nu}_r$ from $\mathbf{Q}_{\mathbf{R}}$
  for all sub-cube $\mathcal{C}_{r_i}$ **do**
    Compute the lower bound $\underline{\nu}_{r_i}$ % Eq. (48)
    if $\mathcal{I}_f.size < 2\underline{\nu}_{r_i}$ **then**
      $\mathbf{R}^* \leftarrow$ `LMOptimization`$(\mathcal{X}_{lin}, \mathcal{Y}_{lin}, \mathbf{R}^*)$
    end if
    Compute the upper bound $\bar{\nu}_{r_i}$ % Eq. (46)
    if $\mathcal{I}_f.size < \bar{\nu}_{r_i}$ **then**
      Add $\mathcal{C}_{r_i}$ to queue $\mathbf{Q}_{\mathbf{R}}$
    end if
  end for
end while
$\mathcal{I}_f$ = `FindCorr`$(\mathcal{X}_{lin}, \mathcal{Y}_{lin}, \mathbf{R}^*)$
return $\mathcal{I}_f, \mathbf{R}^*$

Algorithm 5 TBnB: Translation BnB

Input:
$\mathcal{X}_{lin} = \{(\bar{\mathbf{d}}_{t_i}, \tilde{\mathbf{b}}_{t_i})\},\ (i = 1, \cdots, N)$: Target embeddings
$\mathcal{Y}_{lin} = \{(\bar{\mathbf{d}}_{s_j}, \tilde{\mathbf{b}}_{s_j})\},\ (j = 1, \cdots, M)$: Source embeddings
$\mathcal{C}_{\mathbf{t}}$: Initial $\mathbb{R}^3$ search cube
$\epsilon_{\mathbf{t}}$: BnB threshold
$\mathcal{I}_f$: Correspondences
Output:
$\mathbf{t}^*$: Optimal translation

Set optimal error $e^* = +\infty$
Add initial cube $\mathcal{C}_{\mathbf{t}}$ into priority queue $\mathbf{Q}_{\mathbf{t}}$
while $e^* - \underline{e}_t < \epsilon_{\mathbf{t}}$ **do**
  Read cube $\mathcal{C}_t$ with the lowest lower bound $\underline{e}_t$ from $\mathbf{Q}_{\mathbf{t}}$
  for all sub-cube $\mathcal{C}_{t_i}$ **do**
    Compute the upper bound $\bar{e}_{t_i}$ % Eq. (65)
    if $\bar{e}_{t_i} < e^*$ **then**
      $(e^*, \mathbf{t}^*) \leftarrow$ `LMOptimization`$(\mathcal{X}_{lin}, \mathcal{Y}_{lin}, \mathcal{I}_f, \mathbf{R}^*, \mathbf{t}^*, e^*)$
    end if
    Compute the lower bound $\underline{e}_{t_i}$ % Eq. (63)
    if $\underline{e}_{t_i} < e^*$ **then**
      Add $\mathcal{C}_{t_i}$ to queue $\mathbf{Q}_{\mathbf{t}}$
    end if
  end for
end while
return $\mathbf{t}^*$

9. Analysis on Point-based and Parameter-based Methods

9.1. Measurement Variation of Point-based Registration

In this section, we further analyze how the optimal rotation of point-based cost functions varies with changes in point location. For simplicity, our analysis focuses on 2-dimensional *point-to-line* registration, considering only rotational transformations and assuming measurement points lie perfectly on the model shape without any noise. In this case, the optimal rotation will initially be the identity element. We then examine how the optimal rotation changes as the noise in the points increases.

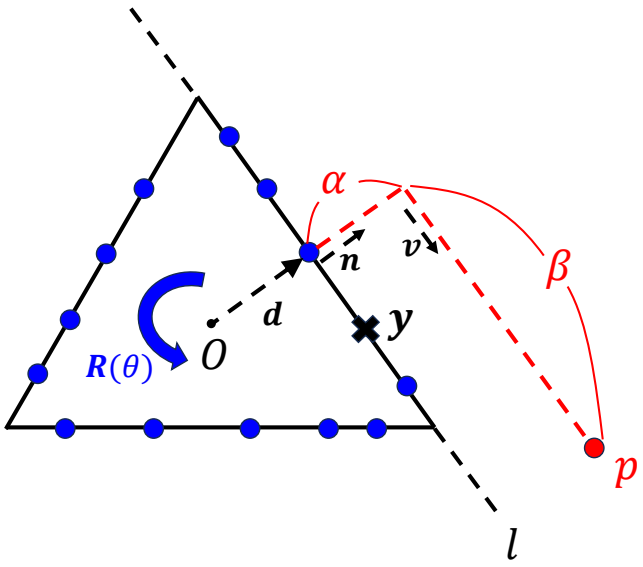

Figure 8. **Measurement points on the model with outlier $\mathbf{p}$.** This figure illustrates measurement points without noise (blue) lying on the corresponding model lines. When an outlier $\mathbf{p}$ (red), expressed by parameters α and β, is paired with line l, the optimal rotation $\mathbf{R}(\theta)$ may adjust to minimize the total *point-to-line* costs.

A measurement point on the model can be written as:

$$\mathbf{p} = \mathbf{d} + \alpha\mathbf{n} + \beta\mathbf{v}, \tag{67}$$

where $\mathbf{d}$ is the displacement of the paired line with the point, $\mathbf{n}$ is the unit-norm displacement (normal vector), α is the noise in the normal direction, $\mathbf{v}$ is the unit-norm direction vector perpendicular to $\mathbf{n}$, and β is the amount of displacement along $\mathbf{v}$. A rotation in $\mathbb{R}^2$ is expressed as an element of $SO(2)$ matrix:

$$\mathbf{R}(\theta) = \begin{pmatrix} \cos\theta & -\sin\theta \\ \sin\theta & \cos\theta \end{pmatrix}. \tag{68}$$

Therefore, as illustrated in Fig. 8, a *point-to-line* distance formulated by $\mathbf{p}$ is:

$$\mathbf{d}_\mathbf{p} = \left|\mathbf{n}^\top \left(\mathbf{R}(\theta)(\mathbf{d} + \alpha\mathbf{n} + \beta\mathbf{v}) - \mathbf{y}\right)\right|, \tag{69}$$

where $\mathbf{y}$ is the given point on the model. Denoting $\mathbf{n} = [n_x, n_y]^\top$, $\mathbf{d} = [d_x, d_y]^\top, \|\mathbf{d}\| = d$, $\mathbf{v} = [v_x, v_y]^\top$, this can be explicitly rewritten as:

$$\begin{aligned} \mathbf{d}_\mathbf{p} &= \left|\left(n_x d_x + n_y d_y + \alpha(n_x^2 + n_y^2) + \beta(n_x v_x + n_y v_y)\right)\cos\theta + \left(\beta(n_y v_x - n_x v_y) + d_x n_y - n_x d_y\right)\sin\theta - \mathbf{n}^\top\mathbf{y}\right| && (70) \\ &= \left|(d+\alpha)\cos\theta + \beta\sin\theta - d\right|. && (71) \end{aligned}$$

If $\alpha = 0$, indicating that $\mathbf{p}$ lies on the paired line, the minimizer θ of the cost is zero, regardless of the value of β. However, if $\alpha > 0$, we observe that absolute value of the minimizer θ decreases as β increases. This aligns with our intuition: a point farther from the center can be slightly rotated to better fit the line. If such outlier points increase, the optimal rotation minimizing the sum of Eq. (69) deviates from the identity. In contrast, adding the number of points with smaller β has no significant effect. This is because substantially increasing θ to align with near outliers would drastically increase the cost associated with inlier points, making the identity matrix the optimal rotation as before.

9.2. Comparison of Curves on Manifold

From the paper, we observed that the sign ambiguity results in two distinct straight lines in the parameter space, which leads to suboptimal solutions. In this section, we investigate how these two lines are mapped as curves on the manifold

and compare the lengths of these curves. First, we represent an element of the Grassmannian $\mathbb{A} \in \mathrm{Gr}(k,n)$ using its unique projection matrix, $\mathbf{P}_{\mathbb{A}} = \mathbf{A}\mathbf{A}^{\top}$, where $\mathbf{A}$ is an orthonormal basis matrix [4]. Then, denoting two tangent vectors at $\mathbf{P} \in \mathrm{Gr}(k,n)$ as $\Delta_1, \Delta_2 \in T_{\mathbf{P}}\mathrm{Gr}(k,n)$, Riemannian metric at the tagent space is defined as:

$$g_{\mathbf{P}}(\Delta_1, \Delta_2) = \frac{1}{2}\mathrm{tr}(\Delta_1 \Delta_2). \tag{72}$$

Given two subspaces $\mathbb{A}, \mathbb{B} \in \mathrm{Gr}(k,n)$ and Riemannian metric of Eq. (72), minimal geodesic equation $\gamma(t)$ connecting two points ($\gamma(0) = \mathbf{P}_{\mathbb{A}}, \gamma(1) = \mathbf{P}_{\mathbb{B}}$) is derived as [3]:

$$\gamma(t) = e^{t\mathbf{C}}\mathbf{P}_{\mathbb{A}}e^{-t\mathbf{C}}, \text{ (where } e^{2\mathbf{C}} = (\mathbf{I} - 2\mathbf{P}_{\mathbb{B}})(\mathbf{I} - \mathbf{2P}_{\mathbb{A}})), \tag{73}$$

Applying this result for connecting two embeddings of affine subspace $\mathbb{A} + \mathbf{c}, \mathbb{B} + \mathbf{d} \in \mathrm{Graff}(k,n)$, Eq. (73) leads to $\gamma : [0,1] \rightarrow \mathrm{Gr}(k+1, n+1)$:

$$\gamma(t) = e^{t\mathbf{C}}\mathbf{P}_{z(\mathbb{A}+\mathbf{c})}e^{-t\mathbf{C}}, \text{ (where } e^{2\mathbf{C}} = (\mathbf{I} - 2\mathbf{P}_{z(\mathbb{B}+\mathbf{d})})(\mathbf{I} - \mathbf{2P}_{\mathbf{z}(\mathbb{A}+\mathbf{c})})), \tag{74}$$

where the length of this geodesic is explicitly given by the root-sum-square of the principal angles between $\mathbf{Y}_{z(\mathbb{A}+\mathbf{c})}$ and $\mathbf{Y}_{z(\mathbb{B}+\mathbf{d})}$.

We now derive the length of the curve mapped from the straight line in the Euclidean parameter space to the manifold. First, we define the mapping between the two spaces as $\phi(\cdot) : \mathbb{R}^m \rightarrow \mathrm{Gr}(k+1, n+1)$, where m is the dimension of the intermediate space (e.g., $m = 4$ for a 3D plane parameter (a,b,c,d)). Then, the mapped curve from the Euclidean embedding is derived as $\phi(t) := \phi(\mathbf{v}(t))$, where $\mathbf{v}(t)$ is the straight line on the parameter space connecting two features represented as $\mathbf{v}_1$ and $\mathbf{v}_2$:

$$\mathbf{v}(t) = t\mathbf{v}_2 + (1-t)\mathbf{v}_1. \tag{75}$$

Then, the velocity at $t = t_k$ is derived by the chain rule:

$$\dot{\phi}(t_k) = (\frac{\partial \phi}{\partial \mathbf{v}}|_{\mathbf{v}=\mathbf{v}(t_k)}) \cdot \dot{\mathbf{v}}(t_k) \tag{76}$$

$$= (\frac{\partial \phi}{\partial \mathbf{v}}|_{\mathbf{v}=\mathbf{v}(t_k)}) \cdot (\mathbf{v}_2 - \mathbf{v}_1). \tag{77}$$

Since an element of Grassmannian is represented by the projection matrix $\phi(\mathbf{v}(t)) \in \mathbb{R}^{(n+1)\times(n+1)}$, the partial derivative yields a 3D matrix $\frac{\partial \phi}{\partial \mathbf{v}} \in \mathrm{R}^{(n+1)\times(n+1)\times m}$. The notation $\cdot$ in Eq. (76) denotes entry-wise multiplication, where (i,j) entry of $\dot{\phi}$ is:

$$\dot{\phi}_{ij} = \frac{\partial \phi_{ij}}{\partial \mathbf{v}} \cdot (\mathbf{v}_2 - \mathbf{v}_1) \tag{78}$$

Then, the length of the curve is approximated by uniformly discretizing $t \in [0,1]$ into N samples:

$$l \approx \sum_{i=0}^{N-1} \sqrt{g_{\phi(i\Delta t)}(\dot{\phi}(i\Delta t), \dot{\phi}(i\Delta t))}\Delta t \tag{79}$$

$$= \sum_{i=0}^{N-1} \frac{1}{\sqrt{2}}\mathrm{tr}(\dot{\phi}^2(i\Delta t))\Delta t, \quad \text{where } \Delta t = \frac{1}{N}. \tag{80}$$

In the case of 2D lines, the embedding is represented by the coordinate $\mathbf{v} = (a,b,c)$ from the line equation $ax+by+c=0$. Then, the corresponding projection matrix $\phi(\mathbf{v}) \in \mathbb{R}^{3\times3}$ in case of $(c < 0)$ is:

$$\phi(\mathbf{v}) = \frac{1}{a^2+b^2+c^2}\begin{bmatrix} b^2+c^2 & -ab & ac \\ -ab & c^2+a^2 & bc \\ ac & bc & a^2+b^2 \end{bmatrix}. \tag{81}$$

Then, each entry of velocity is:

$$\dot{\phi}_{11} = \frac{1}{(a^2+b^2+c^2)^2}\begin{bmatrix}-2a(b^2+c^2) & 2a^2b & 2a^2c\end{bmatrix}\cdot\begin{bmatrix}a_2-a_1 & b_2-b_1 & c_2-c_1\end{bmatrix}^\top \tag{82}$$

$$\dot{\phi}_{12} = \frac{1}{(a^2+b^2+c^2)^2}\begin{bmatrix}-b(b^2+c^2-a^2) & -a(a^2+c^2-b^2) & 2abc\end{bmatrix}\cdot\begin{bmatrix}a_2-a_1 & b_2-b_1 & c_2-c_1\end{bmatrix}^\top \tag{83}$$

$$\dot{\phi}_{13} = \frac{1}{(a^2+b^2+c^2)^2}\begin{bmatrix}c(b^2+c^2-a^2) & -2abc & a(a^2+b^2-c^2)\end{bmatrix}\cdot\begin{bmatrix}a_2-a_1 & b_2-b_1 & c_2-c_1\end{bmatrix}^\top \tag{84}$$

$$\dot{\phi}_{21} = \dot{\phi}_{12} \tag{85}$$

$$\dot{\phi}_{22} = \frac{1}{(a^2+b^2+c^2)^2}\begin{bmatrix}2ab^2 & -2b(a^2+c^2) & 2b^2c\end{bmatrix}\cdot\begin{bmatrix}a_2-a_1 & b_2-b_1 & c_2-c_1\end{bmatrix}^\top \tag{86}$$

$$\dot{\phi}_{23} = \frac{1}{(a^2+b^2+c^2)^2}\begin{bmatrix}-2abc & c(a^2+c^2-b^2) & b(a^2+b^2-c^2)\end{bmatrix}\cdot\begin{bmatrix}a_2-a_1 & b_2-b_1 & c_2-c_1\end{bmatrix}^\top \tag{87}$$

$$\dot{\phi}_{31} = \dot{\phi}_{13} \tag{88}$$

$$\dot{\phi}_{32} = \dot{\phi}_{23} \tag{89}$$

$$\dot{\phi}_{33} = \frac{1}{(a^2+b^2+c^2)^2}\begin{bmatrix}2ac^2 & 2bc^2 & -2c(a^2+b^2)\end{bmatrix}\cdot\begin{bmatrix}a_2-a_1 & b_2-b_1 & c_2-c_1\end{bmatrix}^\top \tag{90}$$

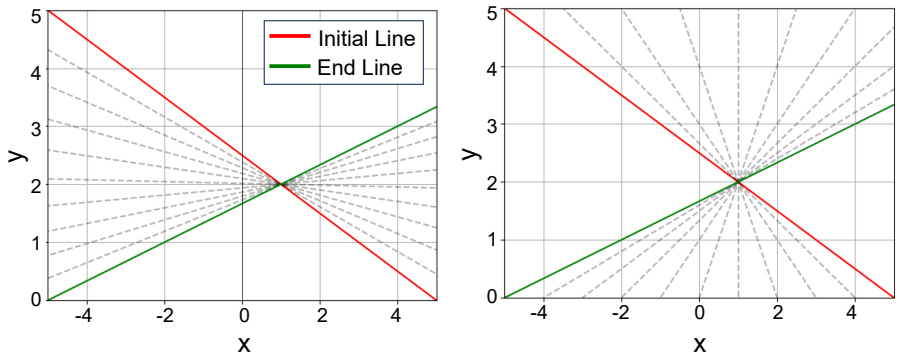

Figure 9. **Comparison of two projected straight lines in parameter space on the manifold.** This figure compares two curves connecting the initial line $\mathbf{v}_1 = (1, 2, -5)$ and the end line $\mathbf{v}_2 = (1, -3, 5)$. The left figure illustrates the projected trajectory of the straight line connecting $(\mathbf{v}_1, -\mathbf{v}_2)$, while the right figure depicts the trajectory of the line connecting $(\mathbf{v}_1, \mathbf{v}_2)$.

Given two lines $x + 2y - 5 = 0$ and $x - 3y + 5 = 0$ represented by $\mathbf{v}_1 = (1, 2, -5)$ and $\mathbf{v}_2 = (1, -3, 5)$, we numerically obtain the length of two curves which connect $(\mathbf{v}_1, \mathbf{v}_2)$ and $(\mathbf{v}_1, -\mathbf{v}_2)$. By defining two straight lines $\mathbf{c}_1(t) = t\mathbf{v}_2 + (1-t)\mathbf{v}_1$ and $\mathbf{c}_2(t) = -t\mathbf{v}_2 + (1-t)\mathbf{v}_1$ on the parameter space, the curve length projected on the manifold is obtained from Eq. (79). The trajectory of each curve is visualized as Fig. 9. From the results by selecting N = 1000, the lengths of two curves, l_1 and l_2 are 2.7539 and 0.3876. This parameter-based approach inevitably selects a specific sign, resulting in different cost terms depending on the selection, as evidenced by their differing lengths. In the case of registering noisy data, this selective overweighing of a specific term may result in a suboptimal solution. In contrast, our cost function consistently minimizes the geodesic distance, effectively avoiding this ambiguity.

An interesting result is that, in every test case, one of the two lines consistently yielded the same length as the geodesic distance, matching to a precision of at least five decimal places and aligning with the trajectory of the geodesic in Eq. (74). Additionally, the sum of l_1 and l_2 always equaled π, which is twice the maximum geodesic distance of $\mathrm{Gr}(2, 3)$, $\pi/2$. From this observation, we can infer that the projections of the two straight lines on the manifold are smoothly connected and form a closed geodesic on $\mathrm{Gr}(2, 3)$ as illustrated in Fig. 10. Assuming $\phi(\mathbf{v}(t))$ and Eq. (73) represent identical curves on the manifold, and factorizing $\phi(\mathbf{v}(t))$ into the same form may reveal interesting properties of the Grassmann manifold and its representation as a projection matrix. This could also lead to an explicit representation of a longer geodesic connecting two points and a closed geodesic equation on the Grassmann manifold.

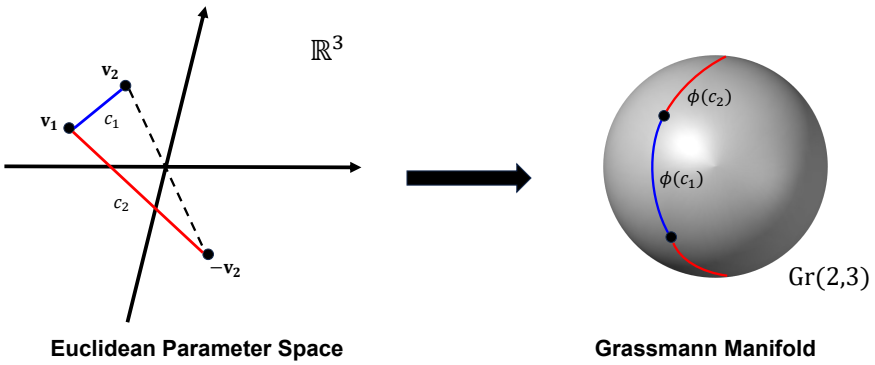

Figure 10. **Mapped straight lines on manifold.** Two distinct straight lines connecting the features, differing only by the sign of one parameter, may form a closed geodesic on the Grassmann manifold. Additionally, the projection of the shorter line (**blue**) may align with the geodesic equation, while the longer line (**red**) is mapped to the longer arc.

10. Experiments Details

10.1. Time Complexity Analysis

In this section, we provide a computational time of experiments in Sec. 5. All the reported times represent the average time required to process a single set. For example, in the object registration experiment, the time for a specific outlier ratio is calculated by dividing the total time taken to compute its 500 sets by 500.

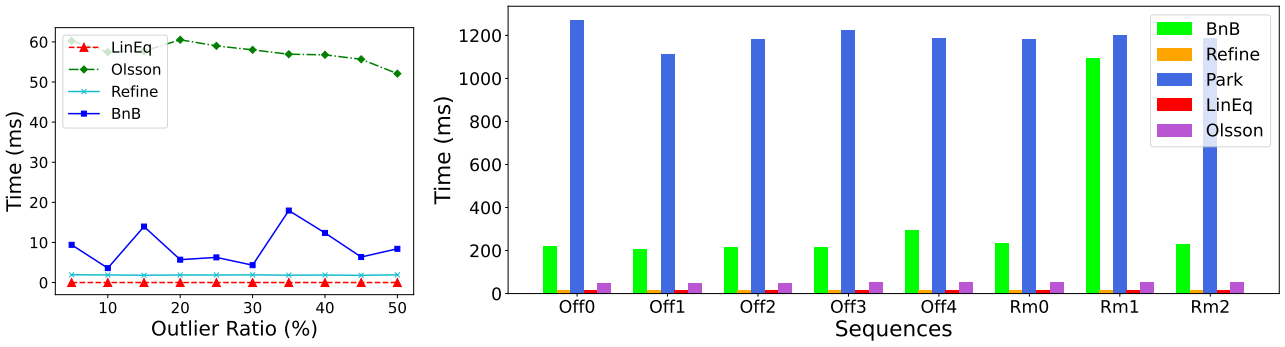

(a) Object registration

(b) RGB-D odometry

Figure 11. **Elapsed time analysis on object registration and RGB-D odometry tasks**. (a) We examine the effect of the outlier ratio on the computational time for the object registration task. We show a comparable computational speed to the approximated parameter-based method while maintaining superior performance. (b) Ours reported reasonable run-time speed for odometry on most sequences.

Object registration task. The result of the object registration experiment is illustrated in Fig. 11a. Noticeably, compared to Olsson's method, which exploits every *point-to-plane* correspondence, both our method and LinEq demonstrated shorter computation times by reformulating the original problem into a plane registration of 13 pairs. LinEq consistently achieved the shortest computation time because the algorithm derives its solution from two consecutive linear equations in the straightforward $\mathbf{Ax} = \mathbf{b}$ form.

RGB-D odometry task. The elapsed time for each sequence in RGB-D odometry experiment is shown in Fig. 11b. Overall, Park's method demonstrated the highest computational time, primarily due to the high resolution of the input images (1200×680) and the computationally intensive point cloud registration necessary to process a large number of points. Our BnB algorithm followed Park's method, showing its highest value in the *Room1* sequence. As mentioned in Sec. 5.2, this exceptionally high value was due to the challenging conditions of this sequence for line matching, as illustrated in Fig. 13. However, compared to the failure of PlückerNet and Olsson in this scenario, our BnB algorithm successfully estimated the optimal pose at the cost of significant computational time.

Table 3. **Elapsed time of 6D chessboard pose estimation using real images.**

	MinPnL [45]	CvxPnL [2]	ASPnL [39]	ASP3L [39]	RoPnL [23]	Refine	Ours
t (ms)	80.91	36.34	0.51	0.62	278.18	1.27	1.24

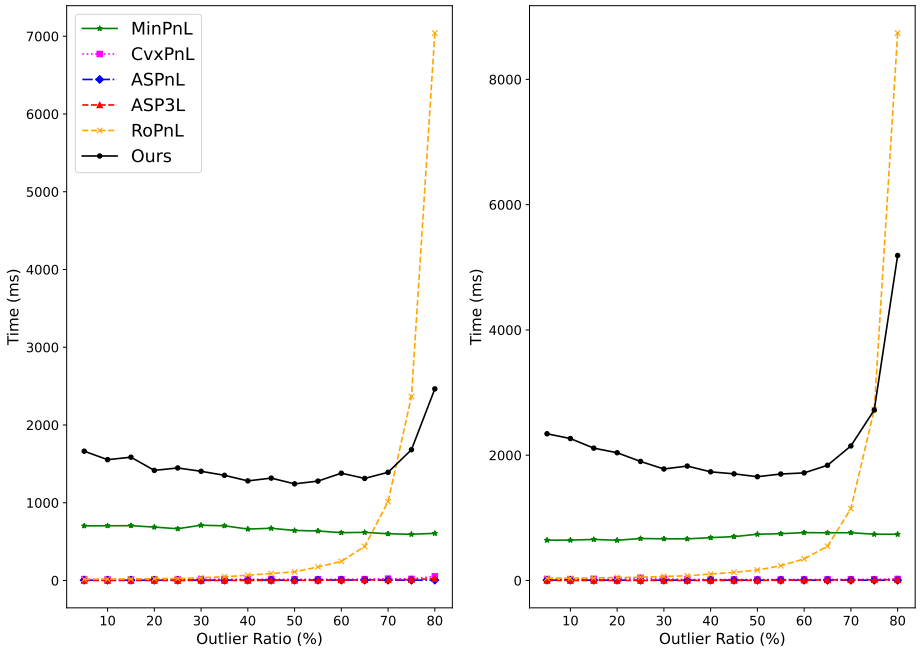

Figure 12. **Elapsed time of PnL experiment with synthetic data**.

PnL task. As shown in Fig. 12, in the synthetic data experiments, both our method and RoPnL showed an increase in computational time as the outlier ratio grew. Overall, RoPnL required less computational time than our method; however, its time increased exponentially with the outlier ratio, taking an average of over 7 seconds at an 80% outlier ratio. In contrast, despite using BnB for calculating translation, our method achieved significantly shorter computation times at high outlier ratios and recorded much lower translational errors, as demonstrated in Sec. 5.3.

In the chessboard experiment, RoPnL exhibited significantly large errors when using the same threshold as in the synthetic experiment, necessitating a reduction in the threshold for a fair comparison. This adjustment resulted in significantly higher computation times for RoPnL as shown in Tab. 3. Additionally, unlike the synthetic experiments that utilized 100 pairs, this real-world experiment employed only 7 pairs, corresponding to the 4×3 chessboard pattern. As a result, we observed a significant reduction in our computation time, making it comparable to the results of ASPnL.

To summarize, as demonstrated in the results of Olsson in the object registration experiment and Park in the RGB-D odometry experiment, algorithms relying on points tend to require significantly more computational time as the number of measurements increases, in contrast to algorithms that compress this information into high-level features. Among these, parameter-based approaches such as LinEq and PlückerNet, which solve linear equations, achieved the shortest computation times but are limited by suboptimal solutions. Overall, our BnB algorithm successfully identified the inlier set and obtained an optimal solution in experiments involving a large number of pairs, particularly those with a high outlier ratio, but required significant computation time. In contrast, experiments with a smaller number of pairs demonstrated significantly shorter computation times. Considering this, the active use of plane features to robustly aggregate redundant lines, along with the selective use of meaningful features, is expected to alleviate these time complexity issues in practical applications.

10.2. Failure Cases in RGB-D Odometry

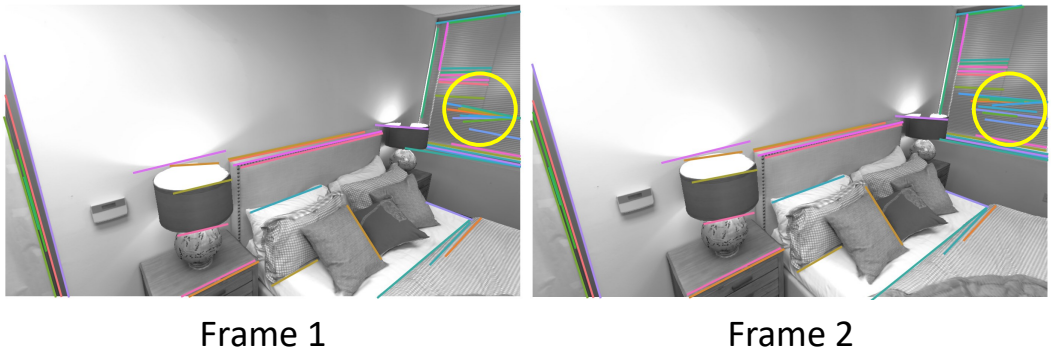

Figure 13. **Failure case of Olsson [29] in *Room1* sequence.**

This section presents visualizations of the frame pairs where each algorithm in the RGB-D odometry experiment recorded the largest error and includes a brief analysis of the causes. As shown in Fig. 13, the areas highlighted with yellow circles reveal frequent failures in line segment matching using GlueStick [32]. In the case of Olsson, which performs convex optimization by considering all correspondences, the algorithm was unable to handle such outliers internally, leading to a complete failure. Although PlückerNet mitigates this issue to some extent using RANSAC, it failed to find the optimal solution in this sequence where the outlier ratio is high.

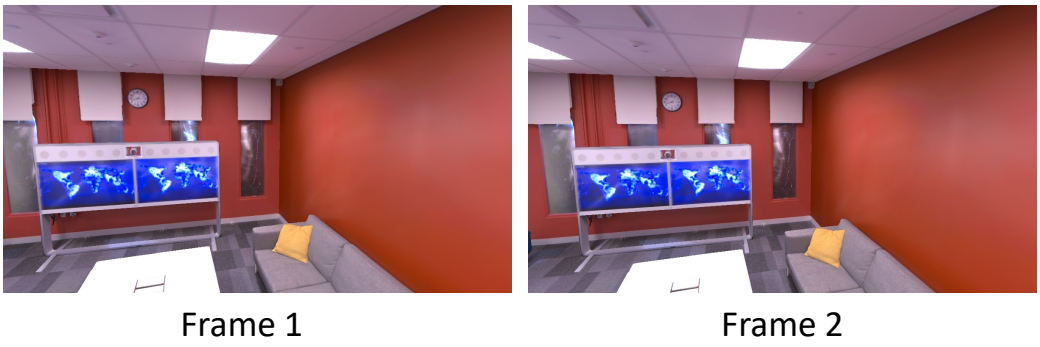

Figure 14. **Failure case of Park [31] in *Office3* sequence** .

Park generalizes the discrete intensity function obtained from the image into a continuous representation in 3D space by utilizing the gradient at a specific point. The gradient is estimated by minimizing the difference between the intensity of the continuous function and that of the discrete function across the neighborhood points. In scenes where the point cloud is dominated by points with the same intensity, as shown in Fig. 14, the objective function exhibits minimal variation with changes in gradient values, leading to erroneous estimation. This gradient leads to incorrect calculations of the intensity function in these regions, resulting in large trajectory errors for the algorithm.